

Deep Feature Statistics Mapping for Generalized Screen Content Image Quality Assessment

Baoliang Chen, Hanwei Zhu, Lingyu Zhu, Shiqi Wang, *Senior Member, IEEE* and Sam Kwong, *Fellow, IEEE*

Abstract—The statistical regularities of natural images, referred to as natural scene statistics, play an important role in no-reference image quality assessment. However, it has been widely acknowledged that screen content images (SCIs), which are typically computer generated, do not hold such statistics. Here we make the first attempt to learn the statistics of SCIs, based upon which the quality of SCIs can be effectively determined. The underlying mechanism of the proposed approach is based upon the wild assumption that the SCIs, which are not physically acquired, still obey certain statistics that could be understood in a learning fashion. We empirically show that the statistics deviation could be effectively leveraged in quality assessment, and the proposed method is superior when evaluated in different settings. Extensive experimental results demonstrate the Deep Feature Statistics based SCI Quality Assessment (DFSS-IQA) model delivers promising performance compared with existing NR-IQA models and shows a high generalization capability in the cross-dataset settings. The implementation of our method is publicly available at <https://github.com/Baoliang93/DFSS-IQA>.

Index Terms—Image quality assessment, screen content image, no-reference, scene statistics, distribution deviation.

I. INTRODUCTION

SCREEN content images (SCIs) have attracted dramatic attention in recent years with the rapid development of digital devices and online communication [1], [2], [3]. The SCI appears in various media, such as electronic books, online news, and screen sharing. Serving as the fundamental technology in SCI compression, exhibition, and processing, assessing the quality of SCI automatically becomes a highly demanding task. In practice, due to the imperfect transmission condition and limited storage space, the quality of SCIs can be degraded by several distortion types. To count for this, numerous methods have been proposed for SCI quality assessment (SCIQA) [4]. According to the availability of reference images, the SCIQA methods fall into two categories: full-reference (FR) SCIQA and no-reference (NR) SCIQA. For FR-SCIQA, the hand-crafted features such as structural features, luminance feature, and Gabor feature are exploited in [5], [6], [7]. With the popularisation of deep learning, the convolutional neural network (CNN) based models have been widely investigated in [8], [9]. For example, Yang *et al.* adopted a fully convolutional network to separate the image into structural regions and texture regions and extracted the structural features and perceptual features from the two

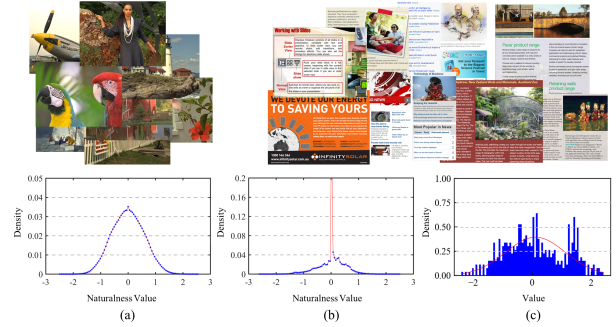


Fig. 1. The statistics of NIs and SCIs. (a) Distribution of Naturalness Values (DNV) of reference images in TID2013 dataset [18]; (b) DNV of reference images in SIQAD dataset [19]; (c) The deep feature statistics of reference images in SIQAD dataset obtained by our proposed method.

regions for SCIQA [9]. Compared with the FR-SCIQA, the NR-SCIQA is more practical in real-world applications. In [10], [11], the quality-aware features including the picture complexity, brightness, sharpness, and textures are adopted. Driven by the hypothesis that human visual system (HVS) is highly sensitive to sharp edges, Zheng *et al.* divided the SCI into sharp edge regions and non-sharp edge regions [12]. Recently, the deep-learning based NR-SCIQA models have shown superior performance by learning the quality-aware features from the data [13], [14], [15], [16], [17]. In particular, Chen *et al.* incorporated a naturalization module in stacked CNNs for quality-aware feature learning [15]. Yang *et al.* proposed a multi-task learning framework that both the distortion types and distortion degrees were analyzed in [17]. However, despite the success of those methods, they usually suffered from the over-fitting problem, presenting an inferior generalization capability, especially in cross-dataset settings.

We believe that the statistics-based methods, which have been proven to be effective for image quality assessment (IQA) of natural images (NIs), become pivotal for SCIs as well. Typically, natural scene statistics (NSS) which have been explored with the assumption that natural images usually hold specific statistical properties and such properties will be corrupted when the images are distorted, are extracted in different domains [20], [21], [22], [23]. As a result, the image quality can be promisingly evaluated by measuring the corruption level. Despite the impressive effectiveness of NSS for NIs, unfortunately, the NSS may not be statistically meaningful for SCIs. As shown in Fig. 1, the distributions of naturalness values [21] of NIs and SCIs presents a stark difference, due to the fact that SCIs are computer generated instead of being acquired by optical cameras. As a consequence, the IQA

B. Chen, H. Zhu, L. Zhu, S. Wang, and S. Kwong are with the Department of Computer Science, City University of Hong Kong, Hong Kong (e-mail: blchen6-c@my.cityu.edu.hk; hwzhu4-c@my.cityu.edu.hk; lingyuzhu-c@my.cityu.edu.hk; shiqiwang@cityu.edu.hk, and cssamk@cityu.edu.hk). Corresponding author: Shiqi Wang.

models designed for NIs usually show a dramatic performance degradation on SCIs [24], [16].

In this paper, we focus on exploring the specific statistics of SCIs in the deep feature domain and developing a generalized NR-SCIQA model. In general, the expected feature statistics should be shared by different image content and be aware of the quality degradation. In this regard, a unified distribution regularization is imposed on the feature space, and the relationship between the image quality and the feature statistics is established by regressing the image quality from the distribution destruction levels. To verify the performance of our method, we conduct both intra-dataset and cross-dataset experiments on two widely used databases, including SIQAD [19] database and SCID [25] database. Experimental results have demonstrated the superior performance of our method in terms of both prediction accuracy and cross-dataset generalization capability. The main contributions of our paper are summarized as follows,

- We propose a novel NR-SCIQA model by exploring the deep feature statistics of SCIs. To the best of our knowledge, this is the first attempt to address the SCIQA from the perspective of learning SCI statistics.
- We regularize the deep features of reference images to obey a multivariate normal distribution, thus the distribution deviation caused by distortion can be efficiently measured by Kullback-Leibler (KL) divergence, without a reference image.
- Extensive experiments demonstrate the effectiveness of the proposed statistics-based method and the superior performance on cross-dataset settings further validates the high generalization capability of our model.

II. RELATED WORKS

A. No-reference Image Quality Assessment

Getting rid of the requirement of reference images in evaluation, the NR-IQA takes an increasingly important role in real-world applications. To obtain the quality-aware feature, the natural scene statistics (NSS) were explored in [26], [21], [20] and thus the distortion could be estimated by measuring the destruction of “naturalness”. In [26], the NSS descriptor was constructed based on the magnitudes and phases of the pyramid wavelet coefficients. The spatially normalized luminance coefficients present a high correlation with image distortion [20] and the image quality could be predicted by the distribution discrepancy. Xue *et al.* exploited the joint statistics of gradient magnitude map and Laplacian of Gaussian response for blind IQA. In [27], [28], the visual codebooks were constructed from local image patches, aiming for the NSS encoding. Moorthy *et al.* proposed a Distortion Identification-based Image Verity and Integrity Evaluation (DIIVINE) model wherein both the distortion identification and quality regression were learned. The singular value decomposition (SVD) was exploited in [29] with the observation that the singular value curve exhibits a high correlation with image blur. Inspired by the free-energy-based brain theory [30], [31], [32], [33], [34] that human visual system (HVS) always attempts to reduce the uncertainty and explains the perceived scene by an internal generative model,

Zhai *et al.* proposed a psychovisual quality metric in [34]. Analogously, Gu *et al.* incorporated the free-energy inspired features and the “naturalness” related features for quality regression [32]. In [35], the saliency map was introduced to guide the quality aggregation due to its high relevance with the semantic obviousness.

Recently, deep learning technologies have achieved great success in various computer vision tasks. In [36], the patch-based NR-IQA model was learned by several CNN layers. This work was extended by DeepBIQ [37], where a pre-trained network is fine-tuned for the generic image description. The multi-tasks including the quality prediction and distortion type identification were explored in [38], aiming for the distortion discrimination capability enhancement. However, the deep-learning based methods are usually suffered from the over-fitting problem, due to the limited size of training data. In [39], [40], [41], [16], the rank information of image pairs was explored which was able to enrich the training samples and mitigate the over-fitting problem to some extent. The generalization performance could also be enhanced by the knowledge transferred from the distortion type identification networks learned from synthesis image databases [42], [43], [16]. In particular, a deep bilinear model was proposed by Zhang *et al.* [42], in which both the pre-trained image distortion classification network and image category classification network were combined for quality regression. In [44], a generalized framework that can be used for both FR and NR IQA tasks was proposed. The meta-learning adopted in [45] presents a superior generalization capability on unseen distortions. Inspired by the free-energy theory, the pseudo-reference information was restored in image-level [46] and feature-level [16], leading to more discriminative feature extraction.

B. No-reference SCI Quality Assessment

Compared with the NIs, SCIs present distinct statistical differences, leading to a dramatic performance drop when the natural IQA models are tested on SCIs. This phenomenon brings a high demand for IQA models designed specifically for SCIs. In [10], the features that represent picture complexity, screen content statistics, global brightness, and sharpness of details were extracted and regressed for SCI quality prediction. Fang *et al.* combined the local-global luminance features and texture features with the assumption that HVS was more sensitive to luminance or texture degradation [11]. In [15], the CNN was introduced with an upsampling layer incorporated, aiming for learning the “naturalization” of SCIs. Inspired by the internal generative mechanism (IGM) theory, Yue *et al.* decomposed the input SCI into predicted and unpredicted portions and learned the quality prediction in an end-to-end manner [47]. As HVS possesses different sensitivity of pictorial and textual regions, a stacked autoencoder was proposed in [48] and the quality-aware feature was extracted in different regions individually. In [49], the statistical features of chromatic continuity and textural variations were extracted and regressed by the support vector regression (SVR). Jiang *et al.* constructed the pseudo global features to alleviate the absence of local quality guidance and a noise classification task was

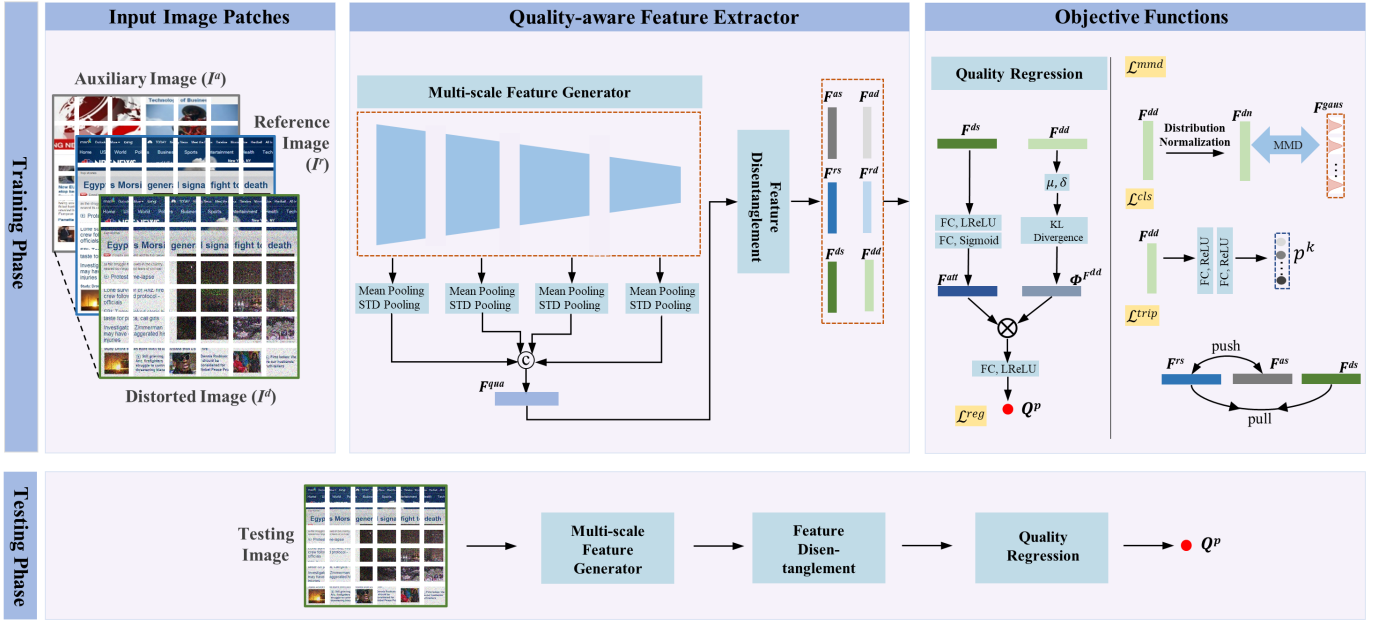


Fig. 2. Illustration of the framework of our proposed method. In the training phase, the images are grouped with a triplet including a reference image (I^r), a distorted image (I^d), and an auxiliary image (I^a). In particular, I^d shares the same content with I^r while its quality is degraded by the distortion. I^a is sampled from pristine images but its content is different from I^r . Then the quality-aware feature of each image is extracted via a multi-scale feature generator and further disentangled into a semantic-aware feature (F^{rs}, F^{ds}, F^{as}) and a distortion-aware feature (F^{rd}, F^{dd}, F^{ad}). We force the normalized distortion-aware feature to obey a unified distribution (F^{gaus}) and treat the unified distribution as the feature statistics shared by the SCIs. As a consequence, the distortion of the I^d can be measured by the feature distribution divergence estimation. Finally, the quality of I^d can be regressed by incorporating both its semantic information (F^{ds}) and distortion information $\Phi^{F^{dd}}$. In the testing phase, only the testing image (without reference) is needed for quality prediction.

learned auxiliarily [50]. Such a multi-task learning strategy was further extended in [17], wherein the identification of both distortion types and distortion levels were learned and incorporated with a quality assessment network. Bai *et al.* proposed the macro-micro modeling of SCIs by constructing a target dictionary. The macro-micro model provided a systematic mathematical interpretation for quality-aware feature extraction [51]. The unified IQA models that are able to assess the quality of both NIs and SCIs also attracted much attention [52], [53]. In particular, Min *et al.* proposed a unified NR-IQA model with a content-adaptive weighting module designed [53]. Recently, the quality assessment transferred from NIs to SCIs was also explored. For example, in [16], the unsupervised domain adaptation was adopted for the quality model transfer from the NIs to SCIs.

III. THE PROPOSED SCHEME

The goal of the proposed method is to determine the quality of the SCIs without reference. The philosophy behind it is comparing the statistics of the input image against the assumed distribution which is regarded to reflect the “naturalness” of pristine SCIs. As such, the perceptual quality of SCIs can be estimated by measuring the destruction of the learned distribution. With those wild assumptions, we propose an NR-SCIQA model by constructing the expected distribution in the deep feature space, thus the quality of test images can be regressed from the distribution deviation. As shown in Fig. 2, our proposed framework consists of image patch sampling, quality-aware feature extractor, and quality regression. More specifically, the image patch sampling aims to obtain fixed-size image patches from the original SCI, thus the model can

be trained and tested when SCIs are of different resolutions. Subsequently, we extract the quality-aware features of each patch based on a multi-stage feature extractor, from which the distortion at different scales can be effectively captured. Herein, the quality-aware feature is expected to contain both the semantic information and distortion information of the input SCI. This is reasonable and its evidence can be exemplified in Fig. 3. From the figure, we can observe that even though the image pairs share the same distortion level, their quality scores can be extremely different, revealing that the image quality is governed by both distortion and content. This phenomenon is also consistent with previous natural IQA works such as [54], [42]. Along this vein, we disentangle the quality-aware feature into a semantic-specific feature and a distortion-aware feature. For the distortion-aware feature, we impose a unified distribution on it and treat the predefined distribution as the feature statistics of SCIs. Regarding the semantic-specific feature, a triplet constraint is adopted based on the underlying principle that the semantic information of the distorted image is similar to the reference image while possessing a large difference from the auxiliary image. Finally, the quality of the distorted SCI can be regressed by synthesizing both the distortion information and semantic information.

A. Triplet Samples for Training

As shown in Fig. 2, we partition the training samples into triplets and each triplet includes a distorted image (denoted as I^d), its corresponding reference image (denoted as I^r), and an auxiliary image (denoted as I^a). In particular, the auxiliary image I^a is randomly sampled from the pristine images



Fig. 3. Distorted SCI sampled from SCID dataset. First row: Images distorted by the motion blur. Second row: Images distorted by the Gaussian noise. The images with the same distortion imposed possess different quality scores due to semantic variance.

while containing a different scene with the I^r . The triplet samples herein aim to disentangle the quality-aware feature into the semantic-specific feature and quality-aware feature which will be elaborated in Sec.III.B. In real-world applications, the spatial resolutions of SCIs can be variant, leading to difficulties in training CNN models at the image-level. As a consequence, we crop all the training images into several patches of identical size. It should be noted that the triplet images are only utilized in the training phase and only a single test image is needed during testing.

B. Quality-aware Feature Extractor

The quality-aware feature extractor consists of two stages including the multi-scale feature generator as well as the feature disentanglement.

1) Multi-scale feature generator. With the input image patches, we design a four-stage based convolutional network for the multi-scale quality-aware feature extraction. Each stage of the generator consists of two convolutional layers and one max-pooling layer. The processing of stage t can be formulated as follows,

$$\mathbf{F}_t^{ms} = f_t(\mathbf{X}), \quad (1)$$

where \mathbf{X} represents the input patch. \mathbf{F}_t^{ms} and f_t mean the output feature map and processing function at stage t . For \mathbf{F}_t^{ms} , we adopt the local mean pooling and local standard deviation (std) pooling to reduce their spatial dimension to 3×3 . The two spatial pooling strategies (mean and std) are widely adopted in the IQA frameworks due to their promising performance in capturing distortion. Subsequently, we concatenate those pooled features as the multi-scale quality-aware feature \mathbf{F}_t^{qua} ,

$$\mathbf{F}^{qua} = f_{mp}(\mathbf{F}_1^{ms}, \mathbf{F}_2^{ms}, \mathbf{F}_3^{ms}, \mathbf{F}_4^{ms}) \oplus f_{sp}(\mathbf{F}_1^{ms}, \mathbf{F}_2^{ms}, \mathbf{F}_3^{ms}, \mathbf{F}_4^{ms}), \quad (2)$$

where f_{mp} and f_{sp} represent the mean pooling and std pooling operation, respectively. \oplus means the concatenation operation which is performed along the channel dimension.

2) Quality-aware feature disentanglement. As we discussed before, human beings rate the image quality governed by both distortion level as well as the scene semantic. To fully exploit the quality feature of \mathbf{F}^{qua} , we disentangle it into a distortion-aware feature and a semantic-specific feature. As shown in Fig. 2, we denote the disentangled semantic representations of I^a , I^r , I^d as \mathbf{F}^{as} , \mathbf{F}^{rs} , and \mathbf{F}^{ds} , respectively and the disentangled distortion representations of I^a , I^r , I^d as \mathbf{F}^{ad} , \mathbf{F}^{rd} , and \mathbf{F}^{dd} , respectively. The disentanglement layer consists of two convolutional layers with the ReLU activation function following each. To ensure the disentanglement of the quality-aware feature \mathbf{F}^{qua} , we first adopt the triplet loss as the objective function with the principle that the semantic features \mathbf{F}^{rs} and \mathbf{F}^{ds} should be similar to each other while both of them are different from the \mathbf{F}^{as} due to the fact that the content shared by I^r and I^d are different from I^a ,

$$\mathcal{L}^{trip} = \frac{1}{B} \sum_{i=1}^B \left[\|\mathbf{F}_i^{rs} - \mathbf{F}_i^{ds}\|_2^2 - \|\mathbf{F}_i^{ds} - \mathbf{F}_i^{as}\|_2^2 + \alpha \right]_+, \quad (3)$$

where i is the input image index in a batch B and α is a margin that is enforced between positive and negative pairs.

For the distortion-aware feature, we impose the Gaussian distribution regularization on the feature space. In particular, each dimension of the distortion-aware feature of the pristine SCIs is expected to obey the standard distribution ($mean = 0, std = 1$) and is independent of each other. In addition, we force the features of the distorted SCIs to share the same distribution except that the means and variances are determined by the distortion. To account for this, we first perform the distribution normalization to the distortion-aware feature \mathbf{F}^{dd} as follows,

$$\mathbf{F}^{dn} = \frac{\mathbf{F}^{dd} - \boldsymbol{\mu}}{\boldsymbol{\sigma} + \epsilon}, \quad (4)$$

where \mathbf{F}^{dn} denotes the normalized results and $\epsilon = 1e - 9$ to avoid zero division error. The $\boldsymbol{\mu}$ and $\boldsymbol{\sigma}$ are the mean and std vectors of \mathbf{F}^{dd} . In particular, supposing N patches are sampled from a distorted image and we denote the μ_j and σ_j as the mean and std values of the j -th dimension of \mathbf{F}^{dd} . The μ_j and σ_j can be formulated as follows,

$$\mu_j = \frac{1}{N} \sum_{n=1}^N (F_{n,j}^{dd}), \quad (5)$$

and

$$\sigma_j = \sqrt{\frac{1}{N-1} \sum_{n=1}^N (F_{n,j}^{dd} - \mu_j)^2}, \quad (6)$$

where the $F_{n,j}^{dd}$ indicates the j -th dimension value of \mathbf{F}^{dd} of the n -th image patch. Through such normalization, the distribution divergence between different distorted SCIs can be mitigated, and the unified distribution regularization is performed by a Maximum Mean Discrepancy (MMD) loss given by,

$$\mathcal{L}^{mmd} = \frac{1}{B} \left\| \sum_{i=1}^B \phi(\mathbf{F}_i^{dn}) - \sum_{i=1}^B \phi(\mathbf{F}_i^{gaus}) \right\|_{\mathcal{H}}^2, \quad (7)$$

where the i indicates the i -th image in a batch and \mathbf{F}^{gaus} is the feature sampled from an independent multivariate normal distribution that shares the same dimensions with \mathbf{F}^{dn} . The ϕ is a function that maps the features into the Reproducing Kernel Hilbert Space (RKHS) [55]. We apply the Gaussian kernel [55] to compute L_{mmd} , such that the distribution discrepancy between \mathbf{F}^{dn} and \mathbf{F}^{gaus} is expected to be minimized. Moreover, for the distortion features \mathbf{F}^{dd} , a distortion type classification loss is further implemented, effectively enhancing the distortion discrimination capability,

$$\mathcal{L}^{cls} = -\frac{1}{B} \sum_{i=1}^B \sum_{k=1}^K y_i^k \log(p_i^k), \quad (8)$$

where i indicates the i -th input image in a batch and p_i^k and y_i^k are its prediction result and ground-truth label of the k -th distortion category.

C. Quality Regression

The quality of the distorted image is regressed by integrating both the semantic information and the distortion information. In particular, the image distortion is estimated by measuring the distribution deviation between the distribution generated by N sampled image patches and the pre-defined multivariate normal distribution. As both the generated distribution and the normal distribution are Gaussian distributions, their deviation can be efficiently measured by the KL divergence as follows,

$$\Phi^{F^{dd}} = -\frac{1}{2} (\mathbf{1} + \log \sigma^2 - \sigma^2 - \mu^2), \quad (9)$$

where μ and σ are mean and std vectors of \mathbf{F}^{dd} acquired by Eqn. (5) and Eqn. (6), respectively. $\mathbf{1}$ is a vector with the same dimension as σ and the value of each dimension is 1. We denote the $\Phi^{F^{dd}}$ as the distortion feature. To explore the relationship between the semantic feature and distortion feature for final quality regression, we use the semantic feature to generate the channel-wise attention for the distortion feature under the philosophy that the different dimensions of the distortion contribute to final quality with different weights and the weights are determined by the image semantic information. Such processing can be described as follows,

$$Q^p = r(\varphi(\mathbf{F}^{ds}) \otimes \Phi^{F^{dd}}), \quad (10)$$

where Q^p is the predicted quality score and the $\varphi(\cdot)$ means the attention generator consists of two fully connected layers with the ReLU and sigmoid as the activation functions, respectively. The \otimes means the point-wise multiplication. The $r(\cdot)$ represents the regression layer, consisting of a fully connected layer and a ReLU layer. Finally, the regressed quality can be supervised by the mean absolute error (MAE) loss as follows,

$$\mathcal{L}^{mae} = \frac{1}{B} \sum_{i=1}^B \|Q_i^p - Q_i^g\|_1, \quad (11)$$

where Q_i^g is the ground-truth quality score of the i -th input image in a batch. In summary, the final objective function of our model is as follows,

$$\begin{aligned} \mathcal{L}^{all} = & \mathcal{L}^{mae} + \lambda_1 \mathcal{L}^{trip} + \lambda_2 \mathcal{L}^{mmd} \\ & + \lambda_3 \mathcal{L}^{cls} + \left(\|\Phi^{F^{rd}}\|_2^2 + \|\Phi^{F^{ad}}\|_2^2 \right), \end{aligned} \quad (12)$$

where the $\Phi^{F^{rd}}$ and $\Phi^{F^{ad}}$ represent the distribution divergence of \mathbf{F}^{rd} and \mathbf{F}^{ad} measured by Eqn. (9). Herein, we minimize their values during training, aiming to persuade them towards a normal distribution. The λ_1, λ_2 and λ_3 are three trade-off parameters.

IV. EXPERIMENTAL RESULTS

In this section, we first present our experimental setup, including the implementation details of the proposed models and benchmarking datasets. Then we compare the proposed method with the state-of-the-art NR SCI-IQA models in both cross-dataset settings and intra-dataset settings. Finally, the ablation study is performed for the functional verification of each module proposed in our method.

1) *Implementation Details*: We implement our model by PyTorch [56]. In the training phase, we crop the image into patches without overlapping with the patch size set by 32×32 . The number of images in a batch is 96, including 32 distorted images, 32 reference images, and 32 auxiliary images (as shown in Fig. 2). We adopt Adam optimizer [57] for optimization. The learning rate is fixed to $1e-4$ with a weight decay set as $1e-4$. The parameters λ_1, λ_2 and λ_3 in Eqn. (12) are set by 1.0, $5e-3$ and 1.0, respectively. We duplicate the samples by 16 times in a batch to augment the data. The maximum epoch is set by 200.

It is worth mentioning that all the experimental pre-settings are fixed in both intra-database and cross-database training. For the intra-database evaluation, we randomly split the dataset into a training set, a validation set, and a testing set by reference images to guarantee there is no content overlap among the three subsets. In particular, 60%, 20%, and 20% images are used for training, validation, and testing, respectively. The experimental results on intra-database are reported based on 10 random splits. To make errors and gradients comparable for different databases, we linearly map the MOS/DMOS ranges of the SIQAD and SCID databases to the DMOS range [0, 100]. Three evaluation metrics are reported for each experimental setting, including Spearman Rank Correlation Coefficient (SRCC), Pearson Linear Correlation Coefficient (PLCC), and Root Mean Square Error (RMSE). The PLCC estimates the prediction linearity and consistency, SRCC measures the prediction monotonicity, and RMSE evaluates the prediction accuracy. Higher PLCC, SRCC, and lower RMSE indicate better performance of the quality model.

2) *SCI Datasets*: The SCI datasets are briefly introduced as follows,

- SIQAD dataset [19] contains 20 reference SCIs and 980 distorted SCIs. The distorted images are derived from seven distortion types including Gaussian Noise (GN), Gaussian Blur (GB), Motion Blur (MB), Contrast Change (CC), JPEG, JPEG2000, and Layer Segmentation based Coding (LSC). For each distortion type, seven distortion levels are generated.
- SCID dataset [25] consists of 1800 distorted SCIs generated by 40 reference images. In this dataset, nine distortion types are involved including GN, GB, MB, CC, JPEG compression, J2K, Color Saturation Change (CSC), High-Efficiency Video Coding Screen Content Compression

TABLE I
QUALITY PREDICTION RESULTS ON CROSS-DATASET SETTINGS. THE TOP TWO RESULTS ARE HIGHLIGHTED IN BOLDFACE.

Training on SIQAD Testing on SCID (SIQAD \rightarrow SCID)								
Method	NIQE	IL-NIQE	BRISQUE	DIIVINE	CORNIA	HOSA	BQMS	SIQE
SRCC	0.2582	0.1015	0.4526	0.4621	0.6904	0.6024	0.6138	0.5822
PLCC	0.3002	0.2601	0.5050	0.4898	0.7097	0.6147	0.6479	0.4788
RMSE	13.5089	13.6750	12.2235	12.3468	9.9777	11.1709	10.7787	10.9275
Method	ASIQE	NRLT	DIQA	WaDIQA	PQSC	RIQA	MtDI	Ours
SRCC	0.6053	0.4851	0.7169	0.6560	0.4744	0.3371	0.6435	0.7669
PLCC	0.6630	0.5367	0.7260	0.6679	0.4908	0.3457	0.6419	0.7815
RMSE	10.9068	11.9496	9.7398	10.5408	12.3392	13.2888	-	8.8366
Training on SCID Testing on SIQAD (SCID \rightarrow SIQAD)								
Method	NIQE	IL-NIQE	BRISQUE	DIIVINE	CORNIA	HOSA	BQMS	SIQE
SRCC	0.3594	0.3197	0.7042	0.7065	0.7925	0.7602	-	-
PLCC	0.3805	0.3857	0.7647	0.7762	0.8062	0.7860	-	-
RMSE	13.2376	13.2065	9.2233	9.0252	8.4682	8.8499	-	-
Method	ASIQE	NRLT	DIQaM-NR	WaDIQaM-NR	PQSC	RIQA	MtDI	Ours
SRCC	-	0.6332	0.7572	0.7881	0.5594	0.5652	0.7611	0.7969
PLCC	-	0.6827	0.7964	0.8267	0.6172	0.5999	0.7437	0.8344
RMSE	-	10.4596	8.5806	7.9832	11.2625	11.4524	-	7.8202

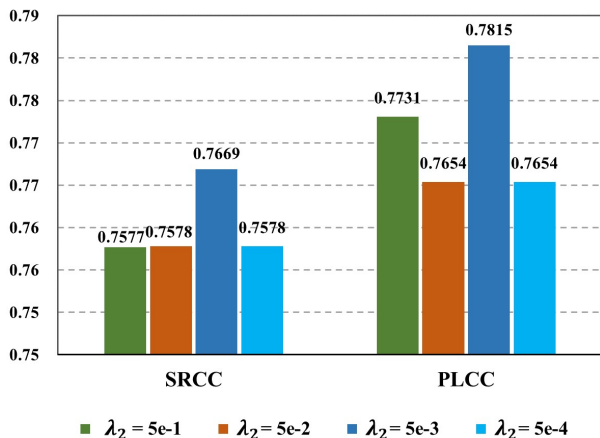


Fig. 4. Study of hyperparameter λ_2 with the cross-dataset setting: SIQAD \rightarrow SCID.

(HEVC-SCC), and Color Quantization with Dithering (CQD). Each distortion type contains five degradation levels. All the SCIs in SIQAD are with a resolution of 1280×720 .

A. Quality Prediction on Cross-database

In this subsection, we first evaluate the performance of our method on the SIQAD and SCID datasets with the cross-dataset settings. Herein, there are two settings: training on the SIQAD dataset and testing on the SCID dataset, and training on the SCID dataset and testing on the SIQAD dataset. These settings are denoted as SIQAD \rightarrow SCID and SCID \rightarrow SIQAD, respectively. There exists a large domain gap caused by the

unshared content, distortion types, and distortion levels between two different datasets, such that the cross-dataset testing appears to be an effective way to evaluate the model generalization capability. We compare the proposed method with both handcrafted feature based methods including NIQE [20], IL-NIQE [58], BRISQUE [21], DIIVINE [23], CORNIA [27], HOSA [59], BQMS [60], SIQE [10], ASIQE [10], NRLT [11], and deep-learning based methods including DIQaM-NR [44], WaDIQaM-NR [44], PQSC [49], RIQA [50] and MtDI [17]. As shown in Table I, most deep-learning based methods achieve inferior performance than the traditional ones, revealing the so-called over-fitting problem. However, our method achieves the best performance in both two settings, demonstrating superior generalization capability that can be learned by the scene statics construction. We also notice that the setting SIQAD \rightarrow SCID is more challenging than the setting SCID \rightarrow SIQAD, as more unseen distortion types are included in the corresponding testing set. Most methods show poor performance on the SIQAD \rightarrow SCID setting with their SRCC scores under 0.7. This can be further verified by the performance comparison of the individual distortion types in Table II. In particular, the distortion types including CC, HEVC-SCC, and CQD in the SCID dataset are unseen when trained on the SIQAD dataset, leading to a significant performance drop compared with on other distortion types. However, our method still achieves superior performance on those distortion types. A consistent phenomenon can be observed in the setting SCID \rightarrow SIQAD. It should be noted that the deep-learning based methods *e.g.*, WaDIQaM-NR usually predicts the image quality by aggregating the cropped patches with score fusion, neglecting the non-local dependency between different local

TABLE II
PERFORMANCE ON INDIVIDUAL DISTORTION TYPES UNDER THE CROSS-DATASET SETTING. THE TOP TWO RESULTS ARE HIGHLIGHTED IN BOLDFACE.

Training on SIQAD and Testing on SCID (SIQAD → SCID)										
Distortion Type		GN	GB	MB	CC	JPEG	J2K	CSC	HEVC-SCC	CQD
CORNIA	SRCC	0.7165	0.8019	0.6903	0.7359	0.6081	0.7324	0.4821	0.1391	0.3372
	PLCC	0.7104	0.8096	0.7049	0.7946	0.6439	0.7423	0.6876	0.2434	0.3825
	RMSE	7.8443	6.8009	7.5681	7.1440	9.1127	11.4375	9.9586	10.8919	12.349
HOSA	SRCC	0.6020	0.6646	0.7383	0.6109	0.4244	0.3944	0.4278	0.1383	0.4844
	PLCC	0.6259	0.7130	0.7606	0.7157	0.4463	0.4427	0.6665	0.3263	0.5206
	RMSE	8.6936	8.1238	6.9275	8.2179	10.6577	15.3051	10.2257	10.6143	11.4112
NRLT	SRCC	0.8604	0.4571	0.6079	0.0721	0.5634	0.4953	0.1370	0.1816	0.1033
	PLCC	0.8602	0.4593	0.6241	0.1284	0.5716	0.5198	0.1896	0.1902	0.1279
	RMSE	6.4094	9.4053	8.5406	8.8774	12.336	13.5911	9.6609	13.6578	12.6803
BQMS	SRCC	0.9437	0.7308	0.5378	0.3548	0.6651	0.5610	0.0064	0.4203	0.3454
	PLCC	0.9499	0.7336	0.5639	0.3896	0.6846	0.5871	0.0106	0.5574	0.4672
	RMSE	3.9298	7.1952	9.0273	8.2443	10.9561	12.8787	9.8524	11.5503	11.3044
PQSC	SRCC	0.8125	0.5365	0.5744	0.4699	0.4407	0.1340	0.0664	0.2960	0.1647
	PLCC	0.8405	0.5741	0.5865	0.5251	0.4753	0.1731	0.1789	0.3442	0.3201
	RMSE	6.8096	8.6898	8.8535	7.6179	13.2403	15.6706	9.6806	13.0619	12.1125
RIQA	SRCC	0.4860	0.4453	0.3380	0.1285	0.0863	0.0031	0.1714	0.2815	0.0802
	PLCC	0.5076	0.4398	0.3626	0.1445	0.1703	0.0061	0.1774	0.2579	0.0554
	RMSE	11.4447	9.0804	7.0662	7.3921	15.9895	16.0320	9.7729	12.8456	12.5659
WaDIQaM-NR	SRCC	0.7360	0.5072	0.4340	0.2490	0.3167	0.4066	0.0063	0.3997	0.2362
	PLCC	0.7706	0.5425	0.5224	0.2667	0.3643	0.4373	0.0479	0.3246	0.3378
	RMSE	8.4676	12.7321	12.9100	12.0870	14.1090	11.8607	10.8595	9.5896	7.4515
DIQaM-NR	SRCC	0.7583	0.6010	0.5972	0.4135	0.5249	0.5891	0.0485	0.3088	0.1754
	PLCC	0.7535	0.6061	0.5945	0.4538	0.5589	0.5941	0.1224	0.2903	0.2694
	RMSE	8.7346	12.0549	12.1741	11.1753	12.5629	10.6091	9.2593	12.3413	7.5421
Ours	SRCC	0.8934	0.8554	0.8122	0.5546	0.8707	0.8495	0.1929	0.5714	0.4957
	PLCC	0.9086	0.8560	0.8186	0.7530	0.8795	0.8623	0.2301	0.5977	0.5429
	RMSE	5.2485	5.4215	6.2779	5.8906	7.1546	8.0560	9.5752	11.1532	10.7369

regions. On the contrary, we construct the quality embedding based on the global distribution descriptors, resulting in more accurate predictions.

B. Quality Prediction on Intra-database

In this sub-section, we first compare our method with several state-of-the-art NR-IQA methods on the SIQAD dataset. The competing models include NIQE [20], BRISQUE [21], QAC [61], IL-NIQE [58], BQMS [60], SIQE [10], ASIQE [10], NRLT [11], HRF [12], CLGF [62], Li *et al.* [63], DIQaM-NR [44], WaDIQaM-NR [44], Yang *et al.* (Tcy20) [48] and Yang *et al.* (TIP21) [64]. The intra-dataset experiment is conducted under ten times random splitting and the median SRCC and PLCC values are reported as final statistics in Table IV. In this table, both the overall performance and the performance of individual distortion types are presented. The top two results are emphasized in boldface. From Table IV, we can observe that our method achieves the best overall performance on the SIQAD dataset in terms of both PLCC and RMSE. The SRCC results are also comparable with the best method WaDIQaM-NR (0.8818 v.s. 0.8834), revealing that the high generalization capability our method could achieve without the sacrifice of intra-dataset performance. In addition, our method presents an effective quality assessment for each individual distortion type as the

distortion-aware features can be learned by measuring the KL-divergence.

To further demonstrate the effectiveness of our method, another experiment is conducted on the SCID database. The experimental results are shown in Table V. From the table, we can observe our method can achieve the best performance and outperform the second-best method by a large margin. In summary, we can conclude that the proposed method is able to predict the quality of SCIs with both high accuracy and generalization capability.

C. Ablation Study

In this subsection, to reveal the functionalities of different modules in our method, we perform the ablation studies on both SIQAD and SCID databases with the cross-dataset setting. More specifically, three main modules are designed in our method including the Gaussian distribution regularization module, the semantic attention module, and the distortion type classification module. As shown in Table VI, we denote the above three modules as “Gaus.”, “Atten.”, and “CLS”, respectively. From the table, we can observe the worst performance is obtained when we ablate the attention module as the semantic-specific feature can adaptively adjust the relationship between the distribution divergence and the quality degradation. In addition, the performance drops again when we ablate the distortion type classification. This phenomenon demonstrates

TABLE III
PERFORMANCE ON INDIVIDUAL DISTORTION TYPES UNDER THE CROSS-DATASET SETTING. THE TOP TWO RESULTS ARE HIGHLIGHTED IN BOLDFACE.

Traininig on SCID and Testing on SIQAD (SCID → SIQAD)								
Distortion Type		GN	GB	MB	CC	JPEG	J2K	LSC
CORNIA	SRCC	0.7675	0.7879	0.6843	0.6606	0.5490	0.6283	0.7023
	PLCC	0.7862	0.8077	0.6805	0.8233	0.5710	0.6405	0.7956
	RMSE	8.0041	8.5575	9.6289	9.4250	7.0041	7.5239	6.0178
HOSA	SRCC	0.7873	0.8334	0.8209	0.4382	0.7013	0.5546	0.7530
	PLCC	0.8179	0.8940	0.8131	0.6987	0.7246	0.5811	0.7756
	RMSE	7.4513	6.5198	7.6502	11.8781	5.8792	7.9733	6.2711
NRLT	SRCC	0.8800	0.6596	0.6091	0.0467	0.7472	0.2663	0.4982
	PLCC	0.8903	0.6653	0.6146	0.0143	0.7511	0.2840	0.5223
	RMSE	6.7920	11.3297	10.2568	12.5773	6.2031	9.9652	7.2758
PQSC	SRCC	0.8540	0.7062	0.4534	0.0431	0.4584	0.4034	0.4024
	PLCC	0.8684	0.7538	0.4504	0.0086	0.4378	0.4833	0.4061
	RMSE	7.3971	9.9724	11.6086	12.5791	8.4482	9.0989	7.7968
RIQA	SRCC	0.6520	0.5627	0.3390	0.0540	0.1250	0.1348	0.0868
	PLCC	0.6873	0.5775	0.3216	0.0985	0.1441	0.1398	0.1581
	RMSE	10.9483	11.6530	10.4261	9.0108	8.8714	11.1871	7.5338
WaDIQaM-NR	SRCC	0.7063	0.6781	0.6271	0.0242	0.1963	0.3399	0.3880
	PLCC	0.7157	0.6922	0.7271	0.0030	0.2060	0.3225	0.4138
	RMSE	9.7918	12.0042	11.1457	8.5756	7.0937	7.8339	5.5437
DIQaM-NR	SRCC	0.6967	0.6298	0.6512	0.2170	0.1219	0.4371	0.0647
	PLCC	0.7109	0.6361	0.7453	0.2391	0.1263	0.3667	0.0489
	RMSE	9.8858	12.8334	10.8240	8.3269	42.6589	7.6998	45.7699
Ours	SRCC	0.8934	0.8433	0.8249	0.4921	0.7158	0.6484	0.6216
	PLCC	0.8999	0.8487	0.8368	0.6954	0.7443	0.6619	0.6480
	RMSE	6.4503	7.9371	7.0185	9.0087	6.3005	7.5920	6.2732

TABLE IV
PERFORMANCE ON SIQAD DATASET UNDER THE INTRA-DATASET SETTING. THE TOP TWO RESULTS ARE HIGHLIGHTED IN BOLDFACE.

Criteria	Distortion	NIQE	BRISQUE	QAC	IL-NIQE	BQMS	SIQE	ASIQE	NRLT	HRFF	CLGF	Li <i>et al.</i>	DIQaM-NR	WaDIQaM-NR	Yang <i>et al.</i> (TIP21)	Yang <i>et al.</i> (Tcy20)	S3QA (Ours)
PLCC	GN	0.8339	0.8346	0.8525	0.7156	0.8377	0.8779	0.8398	0.9131	0.9020	0.8577	0.8957	0.9270	0.9158	0.9139	0.9249	0.9245
	GB	0.5946	0.8359	0.5587	0.5238	0.8739	0.9138	0.9059	0.8949	0.8900	0.9082	0.9164	0.9114	0.8990	0.9225	0.9229	0.9164
	MB	0.2878	0.7666	0.3780	0.4657	0.6733	0.7836	0.7724	0.8993	0.8740	0.8609	0.8679	0.8207	0.8869	0.8948	0.8980	0.8825
	CC	0.3132	0.5489	0.0744	0.1098	0.3146	0.6856	0.6894	0.8131	0.8260	0.7440	0.8129	0.8609	0.8245	0.7772	0.7823	0.8563
	JPEG	0.4591	0.7346	0.3017	0.3296	0.6096	0.7244	0.6756	0.7932	0.7630	0.6598	0.8326	0.7858	0.8491	0.8014	0.8115	0.8383
	J2K	0.3774	0.7645	0.1885	0.4184	0.6358	0.7339	0.6381	0.6848	0.7540	0.7463	0.9279	0.7683	0.8077	0.7984	0.8734	0.7946
	LSC	0.4314	0.6980	0.3367	0.1502	0.4814	0.7332	0.6413	0.7228	0.7700	0.5575	0.7999	0.7536	0.7907	0.7460	0.7844	
	ALL	0.3415	0.7237	0.3751	0.3854	0.7575	0.7906	0.7884	0.8442	0.8520	0.8331	0.8834	0.8799	0.8890	0.8529	0.8738	0.8818
	SRCC	GN	0.8324	0.8665	0.8416	0.7502	0.8347	0.8517	0.8299	0.8966	0.8720	0.8478	0.9075	0.8993	0.9070	0.9102	0.9180
GB		0.6178	0.8234	0.6238	0.5034	0.8591	0.9174	0.9021	0.8812	0.8630	0.9152	0.9150	0.8810	0.8886	0.9223	0.9163	0.8987
MB		0.3921	0.6786	0.3375	0.4253	0.6707	0.8347	0.7765	0.8919	0.8500	0.8694	0.8674	0.8134	0.8588	0.8867	0.8931	0.8675
CC		0.1702	0.7256	0.0745	0.0402	0.2450	0.6874	0.4068	0.7072	0.6870	0.5716	0.7952	0.7745	0.7274	0.7471	0.7785	0.7953
JPEG		0.4467	0.7543	0.1451	0.2745	0.6026	0.7438	0.6624	0.7698	0.7180	0.6778	0.7863	0.7441	0.8027	0.7768	0.8081	0.8142
J2K		0.3558	0.7456	0.1937	0.3880	0.6182	0.7241	0.6241	0.6761	0.7440	0.7681	0.8804	0.7427	0.7608	0.7783	0.8669	0.7499
LSC		0.3953	0.6323	0.1866	0.1535	0.5215	0.7337	0.6216	0.6978	0.7400	0.5842	0.8116	0.7028	0.7786	0.7585	0.7355	0.7510
ALL		0.3695	0.7708	0.3009	0.3575	0.7251	0.7625	0.7570	0.8202	0.8320	0.8107	0.8645	0.8662	0.8780	0.8336	0.8543	0.8820
RMSE		GN	8.2319	7.5643	8.1054	8.4529	8.1451	8.1416	8.0975	6.2678	6.3110	-	-	5.5676	5.9814	5.9745	6.3625
	GB	7.9880	8.4593	7.8821	9.5842	7.3769	6.4239	6.4267	6.7385	6.9170	-	-	6.2084	6.7192	5.7319	5.7767	5.7077
	MB	10.6760	9.4532	10.1330	10.7232	9.6127	8.0783	8.2582	6.4600	6.4520	-	-	6.9046	5.5435	6.7144	5.6846	5.9666
	CC	10.0420	8.6786	12.3041	12.9043	11.9399	9.1565	9.1116	7.8744	7.8430	-	-	6.2280	7.0092	8.0684	7.5985	5.8874
	JPEG	8.7865	5.8643	11.0892	9.4592	7.4485	6.4778	6.9279	5.8625	5.8720	-	-	6.5162	5.2383	6.8006	5.3835	5.7826
	J2K	8.3476	6.1375	10.9169	8.4099	8.0220	7.6727	8.0021	6.5017	6.5440	-	-	6.2439	5.6635	6.5538	4.8967	5.4014
	LSC	7.6972	6.2321	11.4067	7.9421	7.4781	6.3160	6.5465	5.4734	5.7860	-	-	5.6322	5.5285	5.4556	5.8593	5.3568
	ALL	13.4670	8.2565	13.2690	13.9320	9.3456	8.7650	8.8064	7.4156	7.5960	7.9172	-	6.7894	6.7552	7.2817	6.9335	6.6684

that distortion discrimination capability plays an important role in quality prediction. The Gaussian distribution regularization performed based on the MMD loss is ablated in the last experiment. In particular, we directly use the quality feature of F^{qua} for quality regression and distortion type classification. The ablation results on both the SIQAD and SCID datasets reveal the inferiority of the feature-based model when compared with the distribution-based one. The best performance is achieved when all the modules are adopted, demonstrating the three modules contribute to the final performance.

In Fig. 4, to explore the optimal hyperparameter λ_2 , we set

its value to be $5e-1$, $5e-2$, $5e-3$, $5e-4$. We can observe the best performance is achieved when we set the parameter as $5e-3$, and a large value or a smaller one will cause the performance to drop to some extent. The reason may lie in the trade-off between the strong distribution regularization and the variation in image quality.

D. Feature Visualization

To better understand the performance of our method, we visualize the quality relevant features F^{rd} and F^{dd} . More specifically, the model learned on the SIQAD dataset is

TABLE V

PERFORMANCE ON SCID DATASET UNDER THE INTRA-DATASET SETTING.
THE TOP TWO RESULTS ARE HIGHLIGHTED IN BOLDFACE.

Metric	PLCC	SRCC	RMSE
BLINDS-II [65]	0.5851	0.5569	12.6253
NIQE [20]	0.2931	0.2508	13.5401
BRISQUE [21]	0.6004	0.5687	11.6976
NFERM [33]	0.5928	0.5803	11.7647
IL-NIQE [58]	0.2573	0.2436	13.6852
BQMS [60]	0.6188	0.6125	11.1251
SIQE [10]	0.6343	0.6009	10.9483
ASIQE [10]	0.6381	0.6046	10.5873
NRLT [11]	0.6216	0.6092	10.9042
CLGF [62]	0.6978	0.6870	10.1439
DIQaM-NR [44]	0.7086	0.6965	10.3085
WaDIQaM-NR [44]	0.7885	0.7654	8.8189
Yang <i>et al.</i> (TIP21) [64]	0.7147	0.6920	10.3988
Yang <i>et al.</i> (Tcy20) [48]	0.7867	0.7562	8.5949
S3IQA	0.8138	0.8146	8.0125

TABLE VI

ABLATION STUDIES IN TWO CROSS-DATASET SETTINGS.

Setting			SIQAD → SCID		SCID → SIQAD	
Gaus.	Atten.	CLS	SRCC	PLCC	SRCC	PLCC
✗	✗	✓	0.7570	0.7697	0.7966	0.8174
✓	✗	✓	0.7159	0.7217	0.7446	0.7732
✓	✓	✗	0.7210	0.7275	0.7483	0.7841
✓	✓	✓	0.7669	0.7815	0.7969	0.8344

adopted for features extraction, and for each row, we randomly select one dimension of F^{rd} and F^{dd} for their distribution visualization. As shown in Fig. 5, the distributions of F^{rd} and F^{ad} present different mean and std values due to the standard distribution being corrupted by the imposed distortion. In particular, the KL-divergence increases as the distortion becomes severe, revealing that the distribution divergence is able to reflect the distortion levels effectively. From Fig. 5, we can observe that the distortion-awareness exists in different dimensions of the distortion-aware features, revealing that the quality prediction should be an aggregation of the distributions at different dimensions.

V. CONCLUSIONS

In this paper, we propose a novel NR-SCIQA method by constructing the specific statistics of SCIs in the deep feature space. In particular, we first extract the quality-aware feature at multi-scales and disentangle it into the distortion-aware feature and semantic-specific feature. The unified distribution constraint is imposed on the distortion-aware feature, aiming for the construction of the statistics of SCI. Finally, the image quality can be estimated by combining both the distribution information and semantic information. Experimental results have demonstrated the superior generalization capability of our scene statistic-based model, especially in cross-dataset settings. The proposed method sheds the light on the exploration of the intrinsic statistics of SCIs and provides potential guidance for high-quality image generation with computers.

REFERENCES

- [1] S. Wang, L. Ma, Y. Fang, W. Lin, S. Ma, and W. Gao, "Just noticeable difference estimation for screen content images," *IEEE Transactions on Image Processing*, vol. 25, no. 8, pp. 3838–3851, 2016.
- [2] S. Wang, K. Gu, X. Zhang, W. Lin, S. Ma, and W. Gao, "Reduced-reference quality assessment of screen content images," *IEEE Transactions on Circuits and Systems for Video Technology*, vol. 28, no. 1, pp. 1–14, 2016.
- [3] S. Wang, K. Gu, S. Ma, and W. Gao, "Joint chroma downsampling and upsampling for screen content image," *IEEE Transactions on Circuits and Systems for Video Technology*, vol. 26, no. 9, pp. 1595–1609, 2015.
- [4] X. Min, K. Gu, G. Zhai, X. Yang, W. Zhang, P. Le Callet, and C. W. Chen, "Screen content quality assessment: overview, benchmark, and beyond," *ACM Computing Surveys (CSUR)*, vol. 54, no. 9, pp. 1–36, 2021.
- [5] Y. Fang, J. Yan, J. Liu, S. Wang, Q. Li, and Z. Guo, "Objective quality assessment of screen content images by uncertainty weighting," *IEEE Transactions on Image Processing*, vol. 26, no. 4, pp. 2016–2027, 2017.
- [6] Z. Ni, L. Ma, H. Zeng, J. Chen, C. Cai, and K.-K. Ma, "Esim: Edge similarity for screen content image quality assessment," *IEEE Transactions on Image Processing*, vol. 26, no. 10, pp. 4818–4831, 2017.
- [7] Z. Ni, H. Zeng, L. Ma, J. Hou, J. Chen, and K.-K. Ma, "A gabor feature-based quality assessment model for the screen content images," *IEEE Transactions on Image Processing*, vol. 27, no. 9, pp. 4516–4528, 2018.
- [8] Y. Zhang, D. M. Chandler, and X. Mou, "Quality assessment of screen content images via convolutional-neural-network-based synthetic/natural segmentation," *IEEE transactions on image processing*, vol. 27, no. 10, pp. 5113–5128, 2018.
- [9] J. Yang, Z. Bian, Y. Zhao, W. Lu, and X. Gao, "Full-reference quality assessment for screen content images based on the concept of global-guidance and local-adjustment," *IEEE Transactions on Broadcasting*, vol. 67, no. 3, pp. 696–709, 2021.
- [10] K. Gu, J. Zhou, J.-F. Qiao, G. Zhai, W. Lin, and A. C. Bovik, "No-reference quality assessment of screen content pictures," *IEEE Transactions on Image Processing*, vol. 26, no. 8, pp. 4005–4018, 2017.
- [11] Y. Fang, J. Yan, L. Li, J. Wu, and W. Lin, "No reference quality assessment for screen content images with both local and global feature representation," *IEEE Transactions on Image Processing*, vol. 27, no. 4, pp. 1600–1610, 2017.
- [12] L. Zheng, L. Shen, J. Chen, P. An, and J. Luo, "No-reference quality assessment for screen content images based on hybrid region features fusion," *IEEE Transactions on Multimedia*, vol. 21, no. 8, pp. 2057–2070, 2019.
- [13] X. Jiang, L. Shen, G. Feng, L. Yu, and P. An, "Deep optimization model for screen content image quality assessment using neural networks," *arXiv preprint arXiv:1903.00705*, 2019.
- [14] Z. Cheng, M. Takeuchi, K. Kanai, and J. Katto, "A fast no-reference screen content image quality prediction using convolutional neural networks," in *2018 IEEE International Conference on Multimedia & Expo Workshops (ICMEW)*. IEEE, 2018, pp. 1–6.
- [15] J. Chen, L. Shen, L. Zheng, and X. Jiang, "Naturalization module in neural networks for screen content image quality assessment," *IEEE Signal Processing Letters*, vol. 25, no. 11, pp. 1685–1689, 2018.
- [16] B. Chen, H. Li, H. Fan, and S. Wang, "No-reference screen content image quality assessment with unsupervised domain adaptation," *IEEE Transactions on Image Processing*, vol. 30, pp. 5463–5476, 2021.
- [17] J. Yang, Z. Bian, Y. Zhao, W. Lu, and X. Gao, "Staged-learning: Assessing the quality of screen content images from distortion information," *IEEE Signal Processing Letters*, vol. 28, pp. 1480–1484, 2021.
- [18] N. Ponomarenko, L. Jin, O. Ieremeiev, V. Lukin, K. Egiazarian, J. Astola, B. Vozel, K. Chehdi, M. Carli, F. Battisti *et al.*, "Image database TID2013: Peculiarities, results and perspectives," *Signal processing: Image communication*, vol. 30, pp. 57–77, 2015.
- [19] H. Yang, Y. Fang, and W. Lin, "Perceptual quality assessment of screen content images," *IEEE Transactions on Image Processing*, vol. 24, no. 11, pp. 4408–4421, 2015.
- [20] A. Mittal, R. Soundararajan, and A. C. Bovik, "Making a "completely blind" image quality analyzer," *IEEE Signal processing letters*, vol. 20, no. 3, pp. 209–212, 2012.
- [21] A. Mittal, A. K. Moorthy, and A. C. Bovik, "No-reference image quality assessment in the spatial domain," *IEEE Transactions on image processing*, vol. 21, no. 12, pp. 4695–4708, 2012.
- [22] A. K. Moorthy and A. C. Bovik, "A two-step framework for constructing blind image quality indices," *IEEE Signal processing letters*, vol. 17, no. 5, pp. 513–516, 2010.

- [23] Moorthy, Anush Krishna and Bovik, Alan Conrad, "Blind image quality assessment: From natural scene statistics to perceptual quality," *IEEE Transactions on Image Processing*, vol. 20, no. 12, pp. 3350–3364, 2011.
- [24] K. Gu, S. Wang, H. Yang, W. Lin, G. Zhai, X. Yang, and W. Zhang, "Saliency-guided quality assessment of screen content images," *IEEE Transactions on Multimedia*, vol. 18, no. 6, pp. 1098–1110, 2016.
- [25] Z. Ni, L. Ma, H. Zeng, Y. Fu, L. Xing, and K.-K. Ma, "Scid: A database for screen content images quality assessment," in *2017 International Symposium on Intelligent Signal Processing and Communication Systems (ISPACS)*. IEEE, 2017, pp. 774–779.
- [26] H. Tang, N. Joshi, and A. Kapoor, "Learning a blind measure of perceptual image quality," in *CVPR 2011*. IEEE, 2011, pp. 305–312.
- [27] P. Ye, J. Kumar, L. Kang, and D. Doermann, "Unsupervised feature learning framework for no-reference image quality assessment," in *2012 IEEE conference on computer vision and pattern recognition*. IEEE, 2012, pp. 1098–1105.
- [28] P. Ye and D. Doermann, "No-reference image quality assessment using visual codebooks," *IEEE Transactions on Image Processing*, vol. 21, no. 7, pp. 3129–3138, 2012.
- [29] Q. Sang, H. Qi, X. Wu, C. Li, and A. C. Bovik, "No-reference image blur index based on singular value curve," *Journal of Visual Communication and Image Representation*, vol. 25, no. 7, pp. 1625–1630, 2014.
- [30] K. Friston, J. Kilner, and L. Harrison, "A free energy principle for the brain," *Journal of Physiology-Paris*, vol. 100, no. 1-3, pp. 70–87, 2006.
- [31] K. Friston, "The free-energy principle: a unified brain theory?" *Nature reviews neuroscience*, vol. 11, no. 2, pp. 127–138, 2010.
- [32] K. Gu, G. Zhai, X. Yang, W. Zhang, and L. Liang, "No-reference image quality assessment metric by combining free energy theory and structural degradation model," in *2013 IEEE International Conference on Multimedia and Expo (ICME)*. IEEE, 2013, pp. 1–6.
- [33] K. Gu, G. Zhai, X. Yang, and W. Zhang, "Using free energy principle for blind image quality assessment," *IEEE Transactions on Multimedia*, vol. 17, no. 1, pp. 50–63, 2014.
- [34] G. Zhai, X. Wu, X. Yang, W. Lin, and W. Zhang, "A psychovisual quality metric in free-energy principle," *IEEE Transactions on Image Processing*, vol. 21, no. 1, pp. 41–52, 2011.
- [35] P. Zhang, W. Zhou, L. Wu, and H. Li, "Som: Semantic obviousness metric for image quality assessment," in *Proceedings of the IEEE Conference on Computer Vision and Pattern Recognition*, 2015, pp. 2394–2402.
- [36] L. Kang, P. Ye, Y. Li, and D. Doermann, "Convolutional neural networks for no-reference image quality assessment," in *Proceedings of the IEEE conference on computer vision and pattern recognition*, 2014, pp. 1733–1740.
- [37] S. Bianco, L. Celona, P. Napoletano, and R. Schettini, "On the use of deep learning for blind image quality assessment," *Signal, Image and Video Processing*, vol. 12, no. 2, pp. 355–362, 2018.
- [38] L. Kang, P. Ye, Y. Li, and D. Doermann, "Simultaneous estimation of image quality and distortion via multi-task convolutional neural networks," in *2015 IEEE international conference on image processing (ICIP)*. IEEE, 2015, pp. 2791–2795.
- [39] X. Liu, J. van de Weijer, and A. D. Bagdanov, "Rankiq: Learning from rankings for no-reference image quality assessment," in *Proceedings of the IEEE International Conference on Computer Vision*, 2017, pp. 1040–1049.
- [40] Y. Niu, D. Huang, Y. Shi, and X. Ke, "Siamese-network-based learning to rank for no-reference 2d and 3d image quality assessment," *IEEE Access*, vol. 7, pp. 101 583–101 595, 2019.
- [41] Z. Ying, D. Pan, and P. Shi, "Quality difference ranking model for smartphone camera photo quality assessment," in *2020 IEEE International Conference on Multimedia & Expo Workshops (ICMEW)*. IEEE, 2020, pp. 1–6.
- [42] W. Zhang, K. Ma, J. Yan, D. Deng, and Z. Wang, "Blind image quality assessment using a deep bilinear convolutional neural network," *IEEE Transactions on Circuits and Systems for Video Technology*, vol. 30, no. 1, pp. 36–47, 2018.
- [43] K. Ma, W. Liu, K. Zhang, Z. Duanmu, Z. Wang, and W. Zuo, "End-to-end blind image quality assessment using deep neural networks," *IEEE Transactions on Image Processing*, vol. 27, no. 3, pp. 1202–1213, 2017.
- [44] S. Bosse, D. Maniry, K.-R. Müller, T. Wiegand, and W. Samek, "Deep neural networks for no-reference and full-reference image quality assessment," *IEEE Transactions on image processing*, vol. 27, no. 1, pp. 206–219, 2017.
- [45] H. Zhu, L. Li, J. Wu, W. Dong, and G. Shi, "MetalQA: Deep meta-learning for no-reference image quality assessment," in *IEEE Conference on Computer Vision and Pattern Recognition*, 2020, pp. 14 143–14 152.
- [46] K.-Y. Lin and G. Wang, "Hallucinated-iqa: No-reference image quality assessment via adversarial learning," in *Proceedings of the IEEE Conference on Computer Vision and Pattern Recognition*, 2018, pp. 732–741.
- [47] G. Yue, C. Hou, W. Yan, L. K. Choi, T. Zhou, and Y. Hou, "Blind quality assessment for screen content images via convolutional neural network," *Digital Signal Processing*, vol. 91, pp. 21–30, 2019.
- [48] J. Yang, Y. Zhao, J. Liu, B. Jiang, Q. Meng, W. Lu, and X. Gao, "No reference quality assessment for screen content images using stacked autoencoders in pictorial and textual regions," *IEEE transactions on cybernetics*, 2020.
- [49] Y. Fang, R. Du, Y. Zuo, W. Wen, and L. Li, "Perceptual quality assessment for screen content images by spatial continuity," *IEEE Transactions on Circuits and Systems for Video Technology*, vol. 30, no. 11, pp. 4050–4063, 2019.
- [50] X. Jiang, L. Shen, L. Yu, M. Jiang, and G. Feng, "No-reference screen content image quality assessment based on multi-region features," *Neurocomputing*, vol. 386, pp. 30–41, 2020.
- [51] Y. Bai, Z. Zhu, G. Jiang, and H. Sun, "Blind quality assessment of screen content images via macro-micro modeling of tensor domain dictionary," *IEEE Transactions on Multimedia*, vol. 23, pp. 4259–4271, 2020.
- [52] X. Min, K. Gu, G. Zhai, M. Hu, and X. Yang, "Saliency-induced reduced-reference quality index for natural scene and screen content images," *Signal Processing*, vol. 145, pp. 127–136, 2018.
- [53] X. Min, K. Ma, K. Gu, G. Zhai, Z. Wang, and W. Lin, "Unified blind quality assessment of compressed natural, graphic, and screen content images," *IEEE Transactions on Image Processing*, vol. 26, no. 11, pp. 5462–5474, 2017.
- [54] D. Li, T. Jiang, and M. Jiang, "Exploiting high-level semantics for no-reference image quality assessment of realistic blur images," in *Proceedings of the 25th ACM international conference on Multimedia*, 2017, pp. 378–386.
- [55] A. Gretton, K. M. Borgwardt, M. J. Rasch, B. Schölkopf, and A. Smola, "A kernel two-sample test," *Journal of Machine Learning Research*, vol. 13, no. Mar, pp. 723–773, 2012.
- [56] A. Paszke, S. Gross, F. Massa, A. Lerer, J. Bradbury, G. Chanan, T. Killeen, Z. Lin, N. Gimelshein, L. Antiga et al., "Pytorch: An imperative style, high-performance deep learning library," in *Advances in neural information processing systems*, 2019, pp. 8026–8037.
- [57] D. P. Kingma and J. Ba, "Adam: A method for stochastic optimization," *arXiv preprint arXiv:1412.6980*, 2014.
- [58] L. Zhang, L. Zhang, and A. C. Bovik, "A feature-enriched completely blind image quality evaluator," *IEEE Transactions on Image Processing*, vol. 24, no. 8, pp. 2579–2591, 2015.
- [59] J. Xu, P. Ye, Q. Li, H. Du, Y. Liu, and D. Doermann, "Blind image quality assessment based on high order statistics aggregation," *IEEE Transactions on Image Processing*, vol. 25, no. 9, pp. 4444–4457, 2016.
- [60] K. Gu, G. Zhai, W. Lin, X. Yang, and W. Zhang, "Learning a blind quality evaluation engine of screen content images," *Neurocomputing*, vol. 196, pp. 140–149, 2016.
- [61] W. Xue, L. Zhang, and X. Mou, "Learning without human scores for blind image quality assessment," in *Proceedings of the IEEE conference on computer vision and pattern recognition*, 2013, pp. 995–1002.
- [62] J. Wu, Z. Xia, H. Zhang, and H. Li, "Blind quality assessment for screen content images by combining local and global features," *Digital Signal Processing*, vol. 91, pp. 31–40, 2019.
- [63] R. Li, H. Yang, T. Yu, and Z. Pan, "Cnn model for screen content image quality assessment based on region difference," in *2019 IEEE 4th International Conference on Signal and Image Processing (ICSIP)*. IEEE, 2019, pp. 1010–1014.
- [64] J. Yang, Z. Bian, J. Liu, B. Jiang, W. Lu, X. Gao, and H. Song, "No-reference quality assessment for screen content images using visual edge model and adaboosting neural network," *IEEE Transactions on Image Processing*, vol. 30, pp. 6801–6814, 2021.
- [65] M. A. Saad, A. C. Bovik, and C. Charrier, "Blind image quality assessment: A natural scene statistics approach in the dct domain," *IEEE transactions on Image Processing*, vol. 21, no. 8, pp. 3339–3352, 2012.

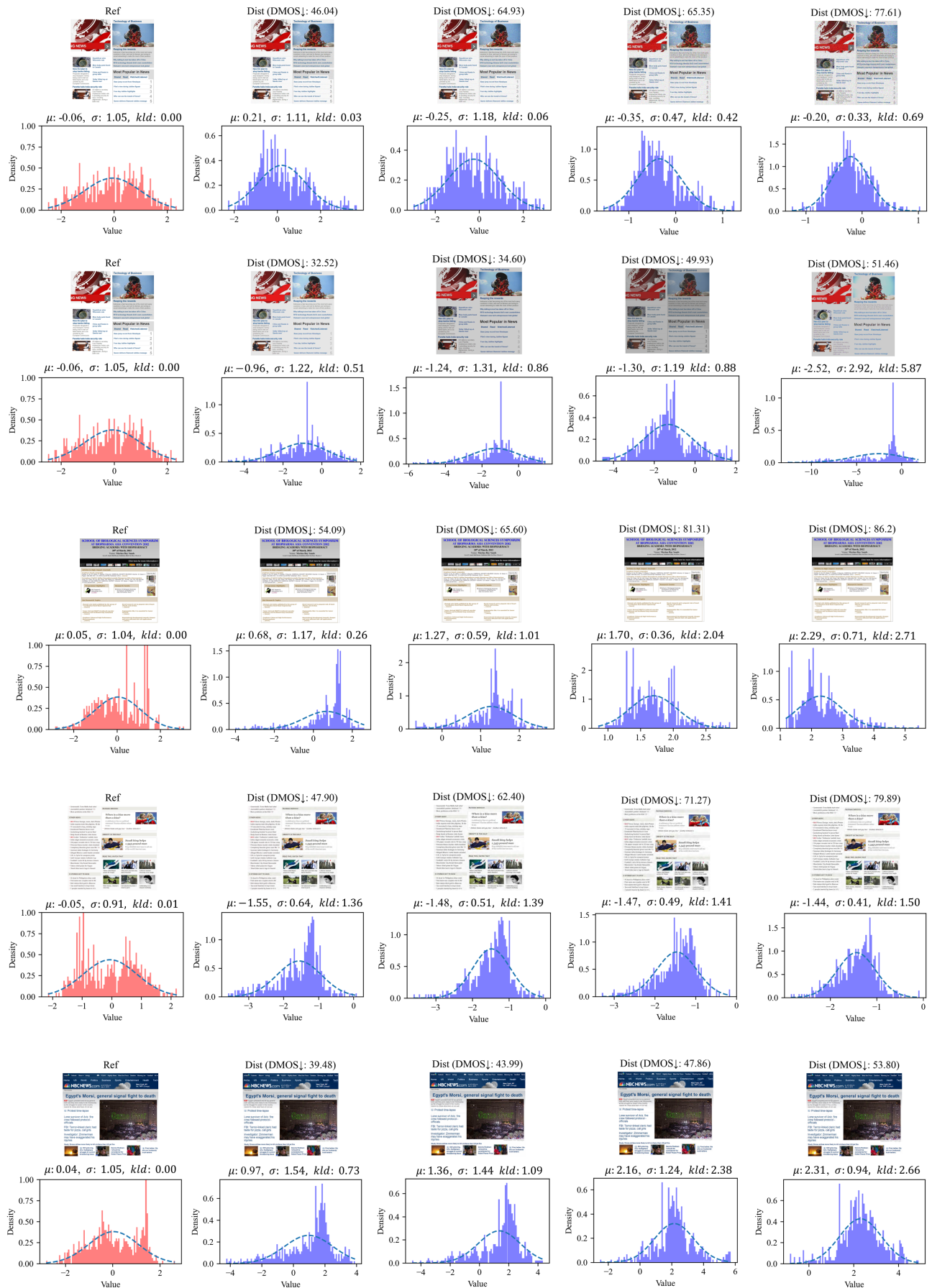


Fig. 5. Feature distribution visualization results. Sub-images in odd rows are the reference images and distorted images. Sub-images in even rows are their corresponding feature distributions. In each row, the same dimension of feature is selected for better comparison. From up to down, the distortion types are Gaussian Noise, Contrast Change, Gaussian Blur, JPEG2000, and Layer Segmentation based Coding. “ μ ” and “ σ ” represent the mean and std of each feature distribution. “kld” means the KL-divergence between the feature distribution and the standard Gaussian distribution. The “↓” means the lower the value the better the quality.